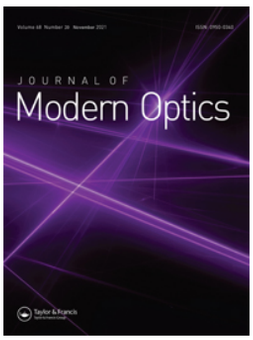

Journal of Modern Optics

ISSN: (Print) (Online) Journal homepage: https://www.tandfonline.com/loi/tmop20

Optical design and fabrication of a three-channel common-aperture multispectral polarization camera

Shan Du, Jun Chang, Chuhan Wu, Yue Zhong, Yaoyao Hu, Xuehui Zhao & Zihang Su

To cite this article: Shan Du, Jun Chang, Chuhan Wu, Yue Zhong, Yaoyao Hu, Xuehui Zhao & Zihang Su (2021) Optical design and fabrication of a three-channel common-aperture multispectral polarization camera, Journal of Modern Optics, 68:20, 1121-1133, DOI: 10.1080/09500340.2021.1977861

To link to this article: https://doi.org/10.1080/09500340.2021.1977861

Published online: 22 Sep 2021.

JOURNAL OF MODERN OPTICS
2021, VOL. 68, NO. 20, 1121–1133
https://doi.org/10.1080/09500340.2021.1977861

Taylor & Francis
Taylor & Francis Group

Optical design and fabrication of a three-channel common-aperture multispectral polarization camera

Shan Du[a], Jun Chang[a,b], Chuhan Wu[a], Yue Zhong[a], Yaoyao Hu[a], Xuehui Zhao[a] and Zihang Su[a]

[a]School of Optics and Photonics, Beijing Institute of Technology, Beijing, People's Republic of China; [b]State Key Laboratory of Applied Optics, China Changchun Institute of Optics, Fine Mechanics and Physics, Changchun, People's Republic of China

ABSTRACT

The ability to detect and recognize the low-contrast and distance targets in a complex environment is of great importance for many applications. However, one or two single spectral channel imaging cannot obtain adequate information. This study reports the design and construction of a common-aperture multispectral polarization imaging system, which can simultaneously obtain visible, short-wave infrared and mid-wave infrared wavebands. Such a system enables the acquirement of spatial, polarization and multispectral information of distance targets simultaneously. The experimental set-up is built to verify the basic principle of the device. The device is used to image optical resolution targets and the car at different times and distances in several complex backgrounds. The generated images are fused by polarization using image processing. The results indicate that the system performs well for imaging low-contrast objects in each waveband.

ARTICLE HISTORY
Received 7 March 2021
Accepted 1 September 2021

KEYWORDS
Optical design; common-aperture; multispectral polarization imaging; polarized fusion

1. Introduction

Multispectral [1–4] and polarization imaging detection, which plays an important role in obtaining the image information of distanced targets, has been widely used to identify the concealed target, geological exploration, mapping, satellite remote sensing, medicine, monitoring and industrial and agricultural production [5,6]. Polarization imaging, given its ability to communicate information about the transverse electric field orientation of an object [7], emphatically characterizes the target's morphology, temperature and material. Therefore, polarization imaging can enhance the contrast between the target and the background [8–10]. Compared with conventional single waveband imaging, multispectral imaging can combine waveband-specific characteristics of objects simultaneously [11]. The images are obtained by multispectral imaging combined with the advantage of visible spectral imaging and infrared spectral imaging. The rich details in the obtained image through the visible optical system detector are easy to observe, and the infrared imaging [12] system can identify the concealed or camouflaged target at night. Therefore, the simultaneous acquisition of multispectral image and polarization image [13,14] is the key to a successful multispectral polarization imaging system [15–19].

In recent decades, some multispectral and polarization imaging systems have been explored in the literature [20–22]. Zhao [20] demonstrated that a multispectral polarization imaging system captured images by rotating a spectral filter and a polarimetric filter. Fu [21] proposed a compressive spectral polarization imaging system consisting of a pixelised polarizer and a coloured patterned detector aligned with a micro-polarizer array. This imaging system requires multiple imaging while rotating the prism. He [22] designed a divided aperture polarization imaging optical system to achieve polarization imaging, of which the spectral band is from 450 to 600 nm. Zhang [16] adopted a non-collinear acousto-optic tunable filter [23] and a linear polarizer to acquire hyperspectral polarization imaging. The spectral band of this system covers the visible to near-infrared region.

Meanwhile, to increase the image detection and recognition probability, most multispectral [24] imaging systems capture images at different wavelengths [17] and fuse the produced images using different image fusion methods [25,26]. For example, the representative schemes in polarization-based dehazing were proposed by Schechner et al. [27–30] who assumed that only airlight is polarized. Ye et al. [31] fused the linear polarization degree diagram and the polarization

CONTACT Jun Chang optics_chang@126.com School of Optics and Photonics, Beijing Institute of Technology, Beijing 100081, People's Republic of China, State Key Laboratory of Applied Optics, China Changchun Institute of Optics, Fine Mechanics and Physics, Changchun 130033, People's Republic of China

angle diagram to obtain the energy characteristic intensity diagram, and the diagram was later enhanced. The enhanced energy characteristic diagram and the image of light intensity were fused by the NSCT method. Thus, we could observe the multispectral wavebands of the target in different backgrounds and observation times.

This study designed and constructed a common-aperture [32] multispectral polarisation camera (CAMPC) to acquire multispectral and polarization optical images simultaneously. The device consists of a common-aperture optical system [24] and three multispectral channel polarization optical systems. Compared with results in some of the literature, such as Mahmoud et al. [5], whose field of view (FOV) is 1°, the common-aperture optical system is used to maintain a wider FOV, whereas three wavebands polarization systems are used to obtain the polarization state of objects in different spectrums. The fused images obtained by image fusion algorithm proposed in the literature [23] possess high-fusion polarization characteristics and contrast. The device enhances the ability to detect the whole system when functioning in the full waveband. Compared with common-aperture single-spectral imaging's insufficiency, the common-aperture multispectral system functions well in full waveband and stabilizes overall system resolution and working distance. A beam-splitter separates light into the visible (VIS, 400–750 nm), short-wave (SWIR, 900–1800 nm) and medium-wave infrared (MWIR, 3500–5500 nm). Visible, SWIR and MWIR light converge on three detectors once they pass different optical systems, and the whole system is calibrated to ensure that the common aperture is coaxial. Finally, we use the device to polarize multispectral images of several objects at different distances and illumination environments and then fuse them. The results indicate that the proposed system's performance is quite satisfactory to obtain clear polarization images in visible, SWIR and MWIR spectrums. Meanwhile, the fusion algorithm combines the advantages of different wavebands and shows that polarization detection can be realized under different backgrounds and illumination conditions.

This study is organized as follows. In Section 2, the multispectral polarizing camera system is designed, and its imaging quality and tolerance analysis are evaluated. In Section 3, The calibration method and experiment of the system are introduced. In Section 4, a simple polarization fusion processing is performed on the obtained images, and the results are discussed and evaluated. Finally, in Section 5, concluding remarks and suggested future directions are provided.

2. Methods

The general polarization cameras are typically designed with a single waveband, such as a visible or infrared spectrum. The single-band polarization imaging reflects the advantages of each band. For example, visible polarization imaging obtains the target's high-intensity image, whereas polarization imaging in the infrared band obtains the contour and radiation of the target in a complex environment and background. Most multispectral devices adopt multiple-aperture and multichannel optical systems to capture the information of the target, thus increasing the size and weight of the whole apparatus. We proposed a common-aperture multispectral system with a larger FOV (4.5°) to realize multispectral polarization imaging to solve the problem. The multispectral system is composed of two beam-splitters and three optical systems. As illustrated in Figure 1, the CAMPC can simultaneously acquire the polarization, spectral and spatial features of an object in three different spectrums.

In Figure 1, The whole system functions in the visible (green light), SWIR (blue light) and MWIR light (red light) wave-bands and employs a common-aperture catadioptric optical system. A Kepler telescope is used in the common-aperture optical system to maintain a wider FOV (4.5°) and enhances the ability to identify the overall system by multiple spectrums. The materials of the common-aperture optical system are ZNS. Meanwhile, the first dichroscope is composed of ZNS. The reflective surface is coated with a dichroic film to transmit light at 400–700 nm, and the transmission surface is coated with an antireflection film to transmit light at 900–1850 nm and 3500–5500 nm. Through the first dichroscope, the object light path into the whole optical system separates

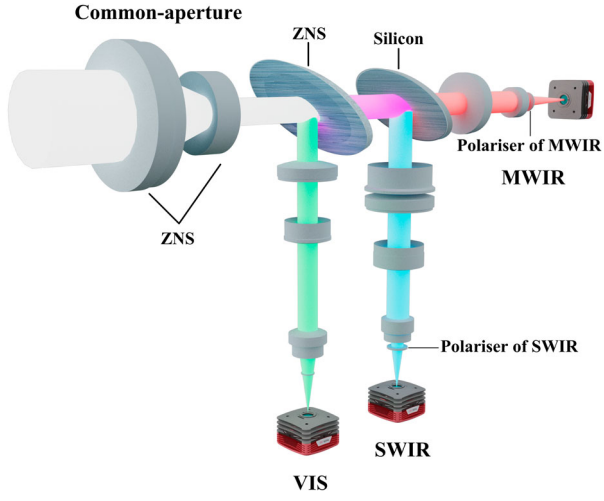

Figure 1. Schematic diagram of common-aperture multispectral and polarization optical imaging system.

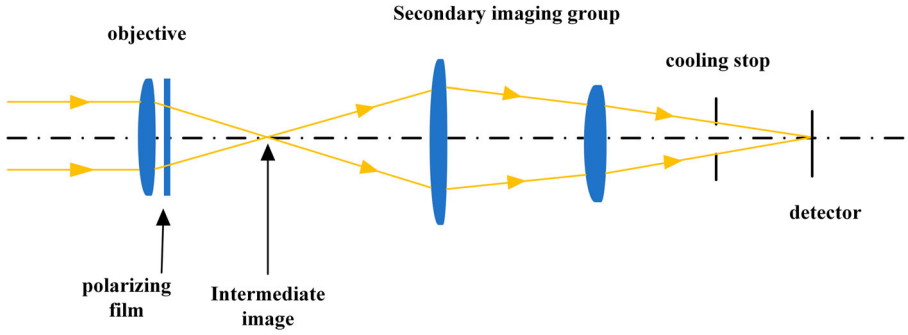

Figure 2. Schematic diagram of the MWIR optical imaging system.

the visible and infrared light with high reflectivity and transmissivity. The reflection ray is imprinted by a set of VIS light lenses onto a visible light focal plane detector, and the transmission light is separated into SWIR and MWIR through the second dichroscope lens. The material of the second dichroic mirror is Silicon, and SWIR light and MWIR light are transmitted by the reflecting surface and the transmitting surface, respectively. These two different wavebands (SWIR and MWIR) are employed in a refractive optical system for secondary imaging. The refractive optical system adopts secondary telescopes, polarizers and objectives to focus the visible, SWIR and MWIR spectrums on the detectors. The common-aperture multispectral and polarization optical imaging system is thus realized. The target is imaged multiple times to obtain the spatial and polarization information in different wavebands simultaneously and fuse the polarization images, increasing identification efficiency.

2.1. MWIR optical system

In this study, the MWIR polarization imaging optical system comprises an objective lens group, a polarizing film and a secondary imaging group. As shown in Figure 2, the incident light first passes through the imaging objective lens and a polarizer to produce an intermediate image, which is then focused onto the secondary imaging group's detector.

The objective lens adopts a secondary telescope to limit the exit beam's aperture diameter and the axial and lateral sizes of the light sequentially. An intermediate image exists between the objective and the secondary imaging group. The effect focal *fM* of the MWIR imaging optical system is given by

$$f_M = F_{MO} \times \beta_M, \tag{1}$$

where F_{MO} is the focal length of the objective lens, and β_M is the magnification of the secondary imaging lens-group. The whole MWIR optical system needs to match

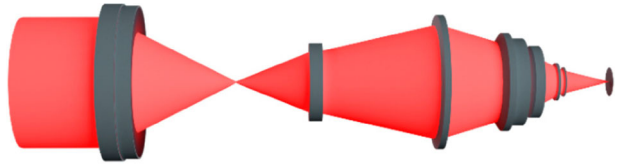

Figure 3. Optical system of the MWIR spectrum.

the cold diaphragm. We design and optimize the final MWIR optical system, as shown in Figure 3.

The modulation transfer function (MTF) plot and point sequence diagram of the acquired MWIR imaging optical system is shown in Figure 4. Figure 4(a) demonstrates that the spot diagram's maximum RMS radius is 8.164 μm, which is less than the minimum pixel size (15 or 25 μm) of a common MWIR detector (GUIDE INFRARED-GAVIN 615A). The MTF curve of the MWIR optical system is close to the diffraction limits illustrated in Figure 4(b).

For the convenience of machining, tolerance analysis on the (MWIR) optical system is carried out. The important tolerance parameters are listed in Table 1. Given that the axial distance between the cold stop and the focal plane of the cooling detector is fixed, the axial distance between the last face of the optical element and the cold stop of the detector is selected as the compensator. MTF is chosen as the tolerance evaluation standard, and the MTF curves through tolerance analysis are shown in Figure 5. The results show that, at the spatial frequency of 40 lp/mm, the probability that the MTF of each field in view is more than 0.45 is 94%, which indicates that the MWIR system meets the technical requirements.

2.2. SWIR optical system

We further limit the diameter of the exit beam. We apply a small polarizer ($\varphi \leq 20$ mm). As shown in Figure 6, the whole optical system relies on a set of objective lenses and a set of relay lenses to project the image on the detector.

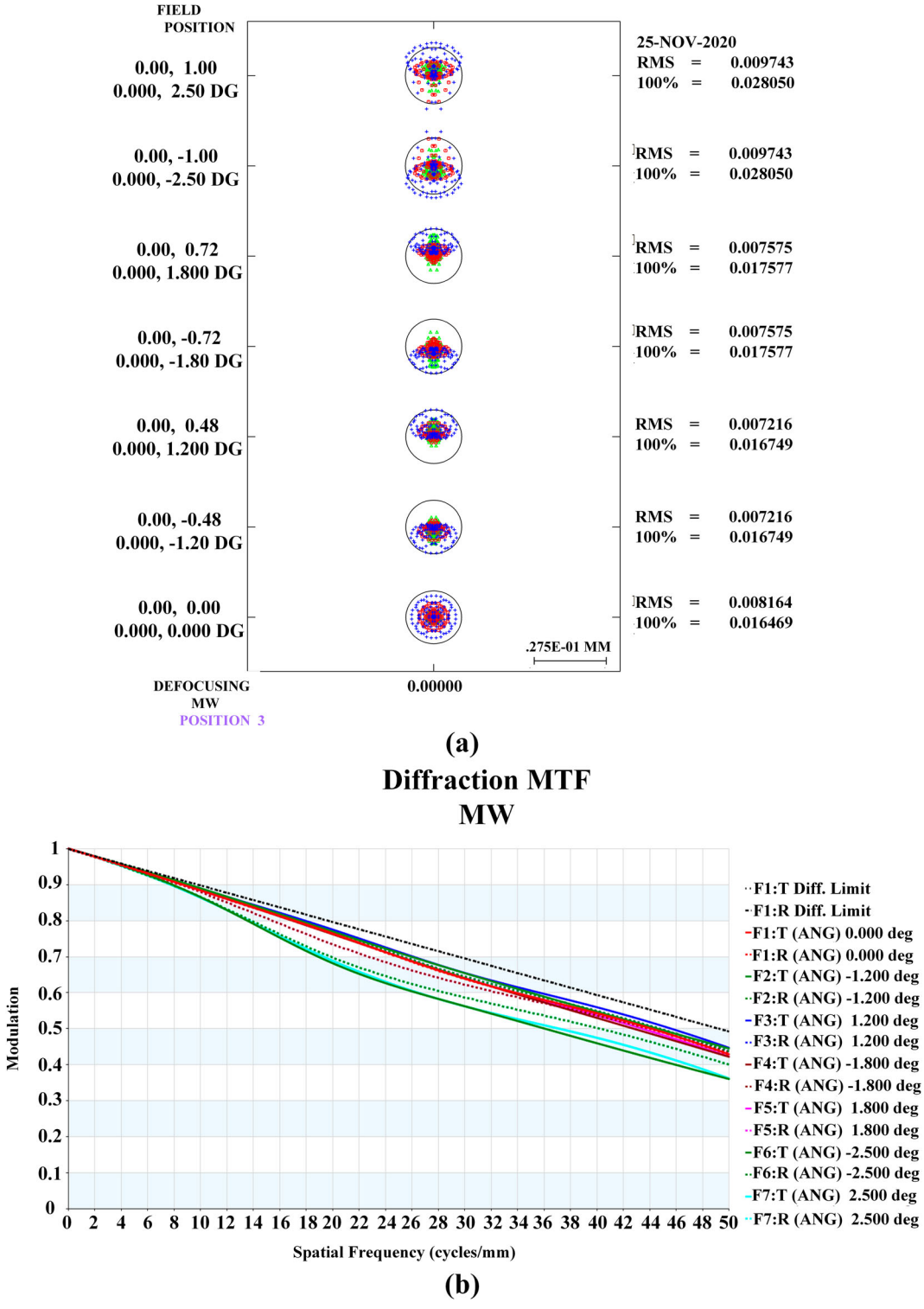

Figure 4. Spot diagram and MTF plots of the MWIR optical imaging system. (a) Spot diagram of the MWIR optical system and (b) its MTF plot.

We reduce the SWIR system's size by designing the primary, intermediate image in the system as a virtual image. The focal length f_{M1} of the SWIR imaging system is given by

$$f_{M1} = F_{SO} \times \beta_s, \tag{2}$$

where F_{SO} is the focal length of the first objective lens, and β_s is the reduction ratio of the relay lens.

Calculation and optimization have been done with the optical system software. The final SWIR optical system is shown in Figure 7. The MTF plots and the spot diagram

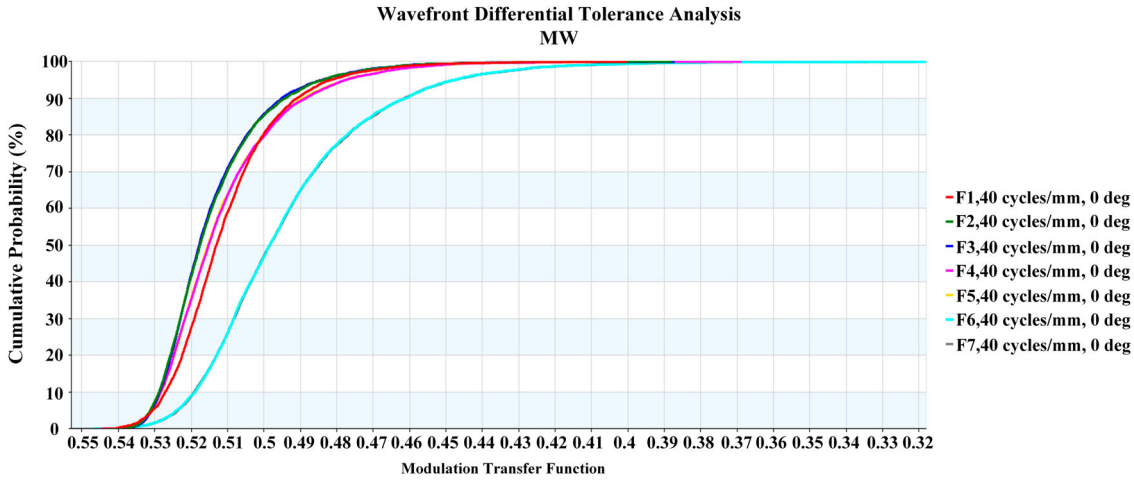

Figure 5. MTF curve for the tolerance analysis of the MWIR system.

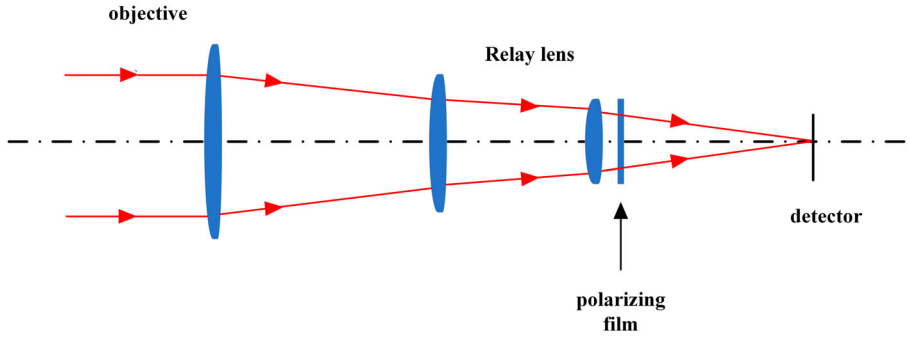

Figure 6. Schematic diagram of the SWIR optical imaging system.

Table 1. MWIR channel tolerance distribution results.

Tolerance classification	Tolerance type	Value
Surface tolerance	Radius	3 Fringes
	Thickness	0.01 mm
	Decenter	0.01 mm
	Tilt	0.8′
	Irregularity	0.5 Fringe
Element tolerances	Decenter	0.02 mm
	Tilt	1′
Others	Index	0.001

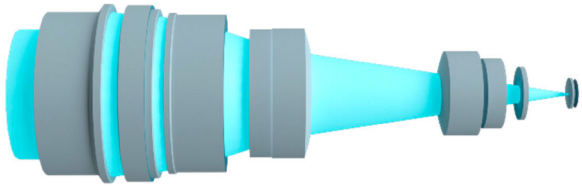

Figure 7. Optical system of the SWIR spectrum.

of this SWIR imaging optical system is shown in Figure 8,

Figures 8(a,b) show that the maximum RMS radius of the spot diagram is 3.56 μm, which is less than the minimum pixel size (15 μm) of the SWIR detector (TKWS638L50001), and the MTF plots of this system are approaching the diffraction limit. The tolerance of this SWIR system is analysed, and the significant tolerance is selected, as shown in Table 2. The axial distance between the last surface of the optical element in the SWIR system and the detector's image surface is selected as the compensator. MTF is selected as the tolerance evaluation standard for tolerance analysis. Figure 9 shows the MTF tolerance analytical curve by Monte Carlo analysis, which indicates the possibility that, in a spatial frequency of 40 lp/mm, the MTF of the SWIR system in different fields is more than 0.68 is 85%.

2.3. *Visible-spectrum optical system*

Similar to that of the SWIR system is the principle of the visible-spectrum optical system, which includes a set of objective lens and relay lens to limit the diameter of the exit beam and the system's length. The visible system designed in this study is combined with the polarization detector to acquire the object's

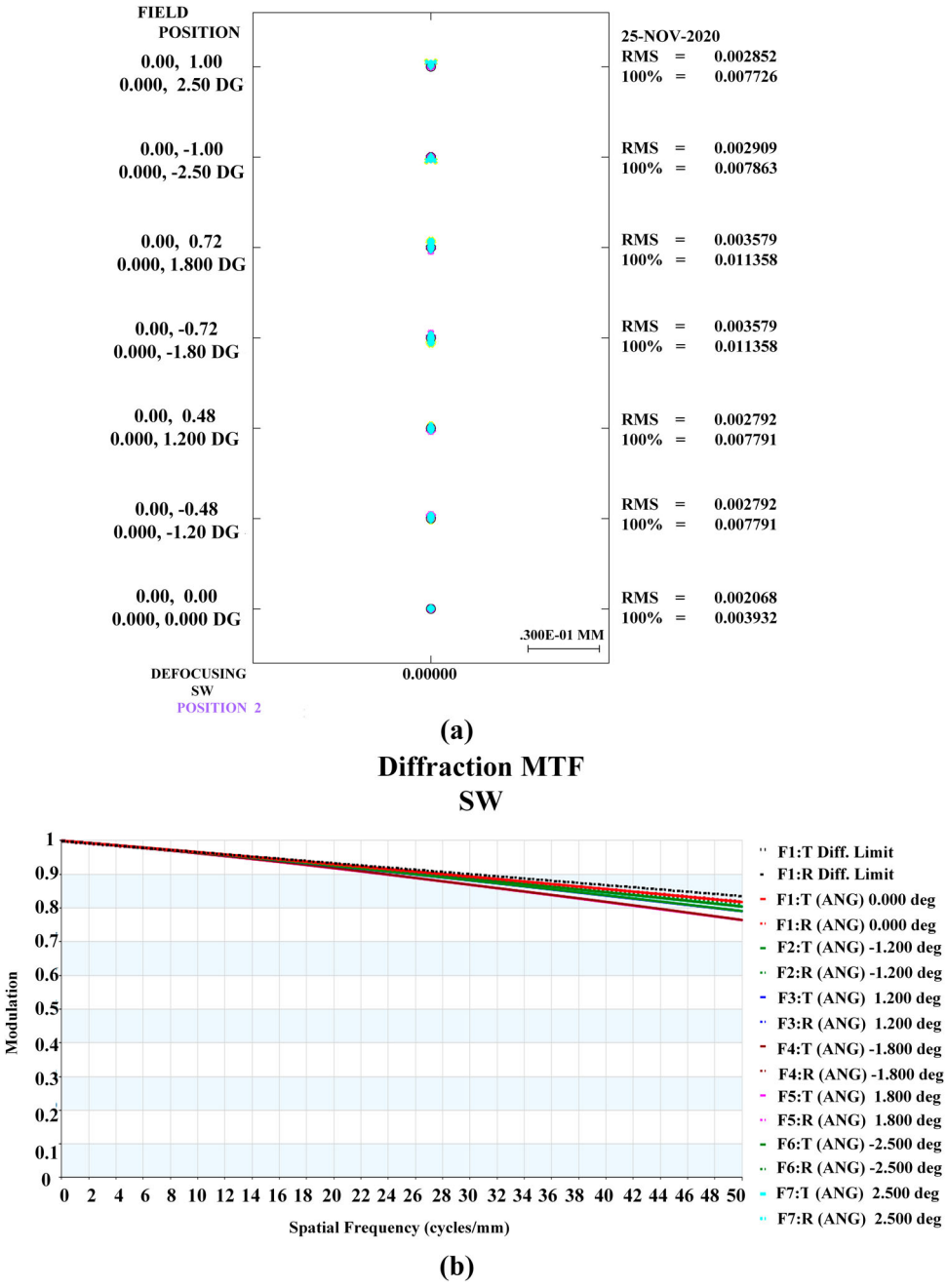

Figure 8. Spot diagram and MTF plots of the SWIR optical imaging system. (a) Spot diagram of the SWIR optical system and (b) its MTF plot.

polarization information simultaneously. The schematic of the optical system is shown in Figure 10. The polarization detector of VIS band (LUCID-TRI050S-P) integrates a set of micro-polarized plates directly into the focal plane array's (FPA) pixels. A 2×2-pixel unit formed by polarizing plates with polarization states of 0°, 45°, 90° and 135° becomes a super pixel. Therefore, the visible polarization imaging system can obtain the polarization information of the target in the four directions of 0°, 45°, 90° and 135° simultaneously in a single frame. The final visible optical system is shown in Figure 11.

Table 2. SWIR channel tolerance distribution results.

Tolerance classification	Tolerance type	Value
Surface tolerances	Radius	2 Fringes
	Thickness	0.01 mm
	Decenter	0.01 mm
	Tilt	1′
	Irregularity	0.5 Fringe
Element tolerances	Decenter	0.02 mm
	Tilt	1′
Others	Index	0.0001

Figures 12(a,b) show the spot diagrams and the MTF plots of the whole visible-spectrum optical system at a full FOV of 4.5°.

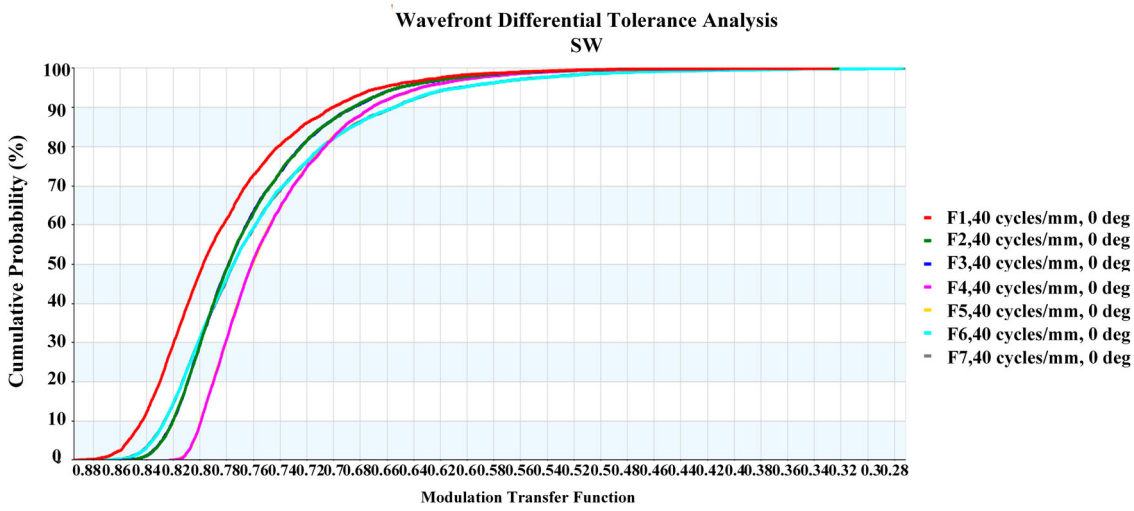

Figure 9. MTF curve for the tolerance analysis of the SWIR system.

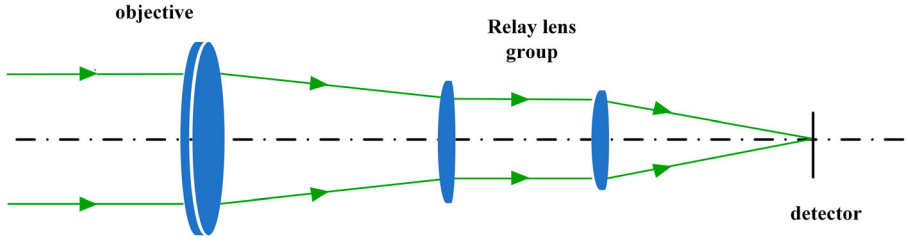

Figure 10. Schematic diagram of the visible-spectrum optical imaging system.

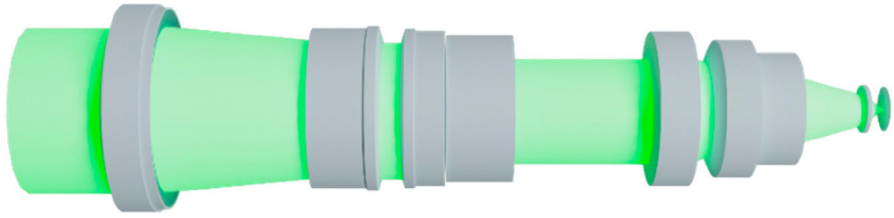

Figure 11. Optical system of the visible spectrum.

The spot diagram's maximum RMS radius is 2.12 μm, which is less than the minimum pixel size (5 μm) of a visible light detector. The MTF plots of visible waveband are close to the diffraction limits. These characteristics satisfy the manufacturing requirements.

Table 3 details the important tolerance parameters selected of the visible optical system. In Figure 13, the MTF of each field of the view tolerance analysis has an 80% probability of more than 0.6 when the spatial frequency is 100 lp/mm, indicating that the visible light system can meet the processing and adjustment conditions.

2.4. Polarizer

The polarizer of the SWIR (THORLABS-LPNIR100) and the polarizer of the MWIR (THORLABS-WP50LM-IRA) are the key components of the polarization imaging systems. The polarisres of the SWIR and MWIR are located between the objective and a set of relay lens. We could capture the polarization information of objects with different polarization states by rotating the angles of the polarizers. The diameters and incident angles of the polarizers are supposed to be controlled because the diameters are generally less than 20 mm and the accepted angle values are often within 4.5°.

2.5. Fusion algorithm

Generally speaking, the fusion algorithm we used here is mainly based on stokes and the degree of polarization images solved with different polarization azimuths. In this algorithm, the fusion process involves three steps: (1) we use VIS, SWIR and MWIR spectral cameras to image

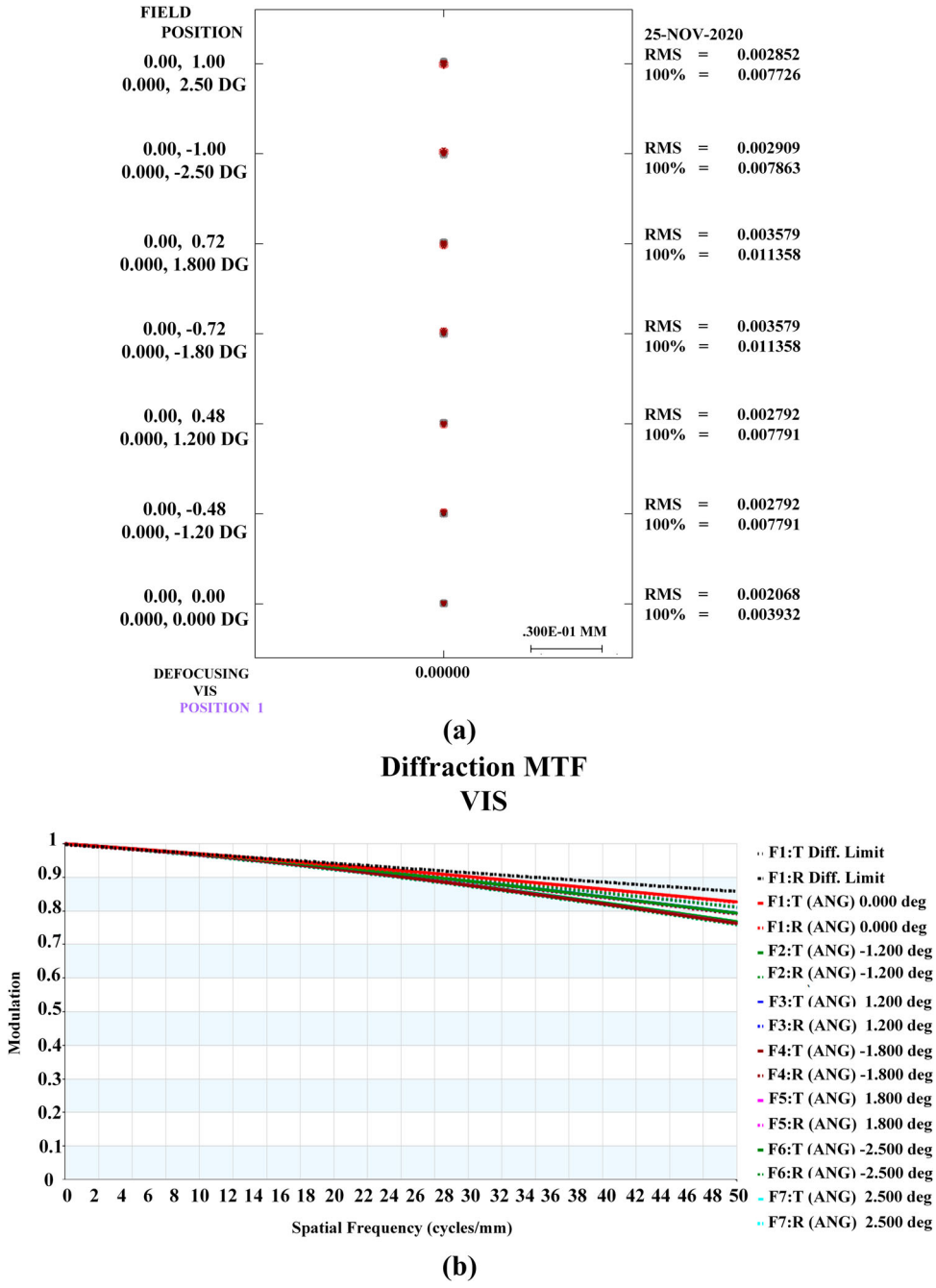

Figure 12. Spot diagram and MTF plots of the visible-spectrum optical imaging system. (a) Spot diagram of the visible-spectrum optical system and (b) its MTF plot.

objects in four different polarization states of 0°, 45°, 90° and 135°. The VIS camera affords the information of the polarization and the highest resolution. The high-frequency information and details of the VIS images are extracted. (2) The SWIR polarization images are used to restrain the information of complicated background and retain the targets' profile details. The processed SWIR images are combined with the VIS images. (3) The MWIR polarization images provide the infrared characteristics of the objects. With the restrained background information, the infrared characteristic is extracted, and the MWIR characteristic images and a fused image of VIS and SWIR are fused.

3. Prototype and experiment

To validate that the multiple-spectrum polarization imaging can enhance the ability to detect objects at different distances and times, we designed and fabricated a prototype in accordance with the optical design theory

Table 3. VIS channel tolerance distribution results.

Tolerance classification	Tolerance type	Value
Surface tolerances	Radius	2 Fringes
	Thickness	0.01 mm
	Decenter	0.01 mm
	Tilt	1′
	Irregularity	0.5 Fringe
Element tolerances	Decenter	0.02 mm
	Tilt	1′
Others	Index	0.0001

in Section 2. The prototype is shown in Figure 14. To guarantee this system's common aperture, we calibrated the coaxiality of the multiple-spectrum camera through a blackbody radiation, a quartz-halogen lamp source, an object target, and a collimator. Then, the coaxiality of the common aperture of the device is calibrated. In Figure 15, the experimental set-up was built to validate that the common-aperture multispectral polarization camera is coaxial.

As shown in Figure 15, the experiment equipment consists of a CAMPC, a blackbody radiation source with power regulating equipment, a set of parallel light tubes and the calibration target. When the common-aperture camera images the target, we can observe whether the target's coordinates are the same on the target surface of the VIS-band, SWIR and MWIR detectors. The blackbody light source with different powers can be detected at different infrared wave-bands, and the quartz-halogen lamp is used as a light source in the visible band. The power of the quartz-halogen lamp is fixed, adjusting the power of the blackbody light source, which can be detected at different infrared wave-bands. The calibration target is the object detected by the prototype. The parallel light tube is used to simulate the infinite distance of the object target.

Figure 16 shows the calibration result and exhibits the images obtained in different directions in blackbody and quartz-halogen lamp light sources. In these images, the object target is imaged in different directions on three detectors because the detector's array format with VIS band is 2448×2048, whereas the array format of the SWIR and the MWIR detectors are 640×512. The number of pixel lines of visible light detectors is 3.825 times those of SWIR and MWIR detectors, and the number of rows is four times those of SWIR and MWIR detectors. Thus, we chose one point from each VIS band image as reference, and (906, 1004) and (940, 1232) are the coordinates. The coordinates of the points in the images in SWIR and MWIR are (237, 251), (231, 252), (246, 308) and (240, 309). The line pixel coordinates of the two points on the MWIR images floated six pixels in contrast with the line pixel of VIS spectral detector. The difference between pixels is within the acceptable error range of practical application and with the row pixel coordinates.

The coordinate on the VIS images is four times those of the SWIR and MWIR images, which means the common-aperture multispectral polarization camera can achieve the coaxial on three spectral waveband systems.

4. Results and discussion

In our experiments, to verify the CAMPA's detecting ability, we performed two different objectives imaging in different backgrounds to verify the CAMPA's basic principle. After processing the detected pictures by polarimetric dehazing algorithm and multispectral fusion algorithm, the experimental results compare the fusion images with the original images, as shown in Figure 17.

We obtained the VIS channel's unpolarized image by reverse calculating the VIS polarization picture, as shown in Figure 17(a). From Figure 17(a), the VIS camera is used to snap the intensity and detailed information of the optical target (1×1.2 m), but the contour information of the object is not obvious under low illumination conditions. Meanwhile, the picture of different polarization states was fused, captured by the VIS camera, as shown in Figure 17(b). The SWIR and MWIR cameras are used to snap polarized infrared information with the same resolution. In Figure 17(c,d), we used polarization dehazing and a single spectral channel fusion algorithm to enhance the optical target images' contrast in short- and mid-infrared wavebands. Figure 17(e) demonstrates the final picture through the multispectral polarization fusion process. The target's fusion image has the same VIS spectral high intensity, good SWIR restraining ability, and MWIR characteristics. The information of high spatial frequency is retained, and the contrast has been enhanced.

The experimental set-up is shown in Figure 17(f–j) is designed to image a car at a 1300-m distance and a complicated background. The CAMPA captures the car images in several spectral channels and different polarisation states. Figure 17(f) shows the unpolarized image of a car 1300-m away in the forest background by reverse calculating the polarization picture with the VIS lens group. In Figure 17(g), this image of the polarization captured in the VIS channel is used to determine the intensity and high-resolution information. In Figure 17(h–i), the car in the distance is excessively small to make out the outline's details. However, the MWIR and SWIR spectral polarization lens group are used to identify the target's infrared characteristic in a complex environment. Figure 17(g–i) illustrates the polarization images by the single waveband fusion algorithm. Figure

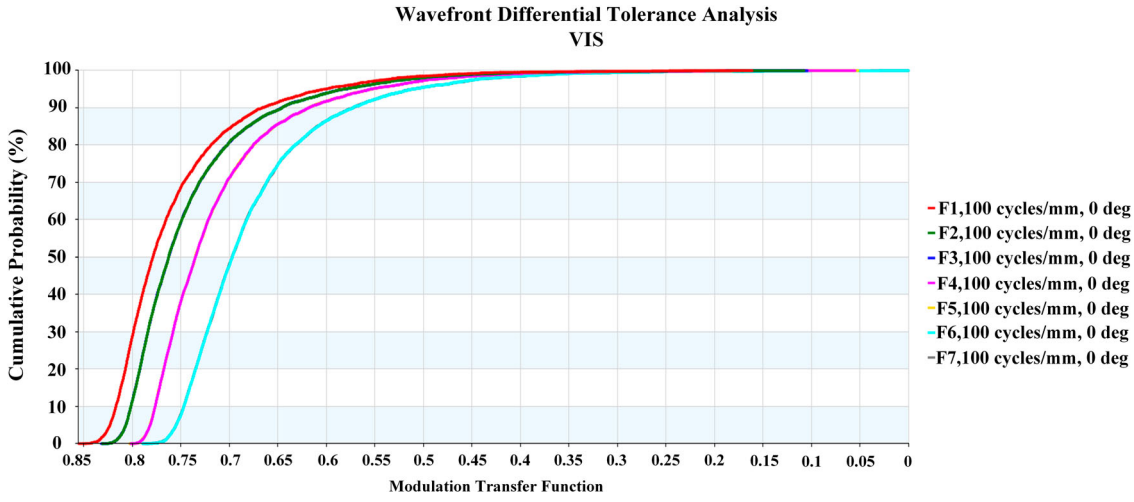

Figure 13. MTF curve for the tolerance analysis of the VIS system.

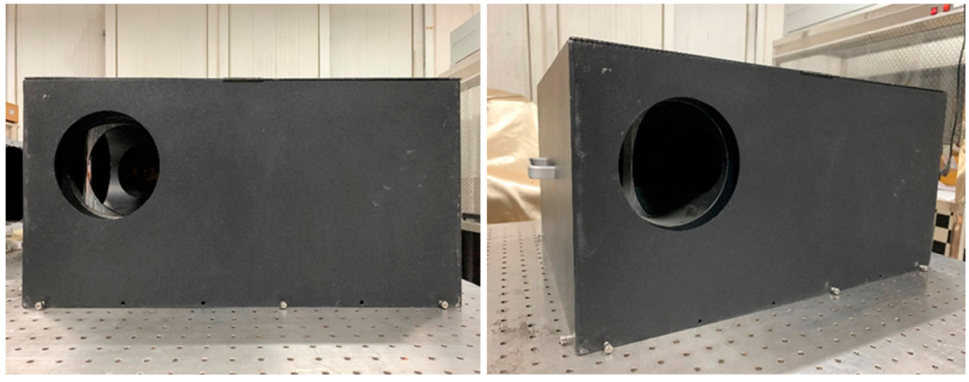

Figure 14. Multiple-spectrum common aperture polarization imaging prototype.

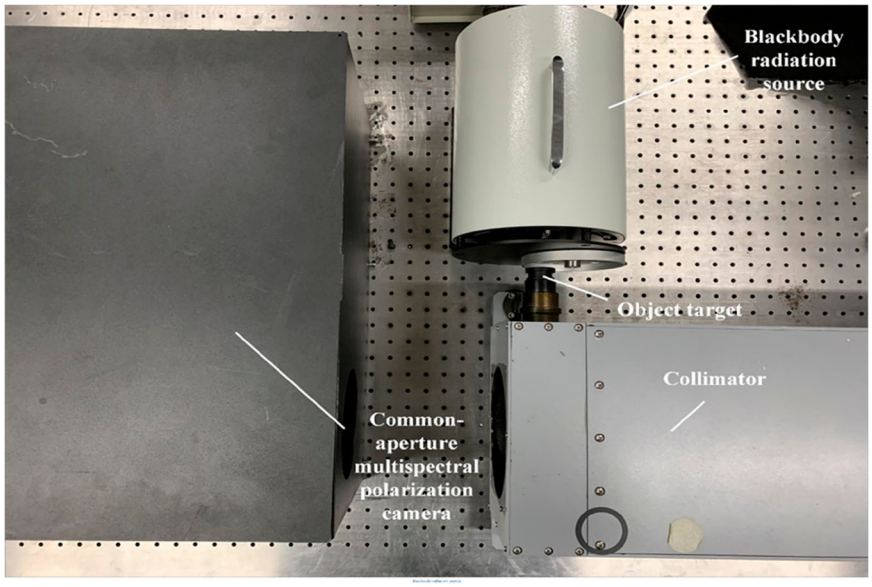

Figure 15. Coaxial calibration experiment for common aperture equipment.

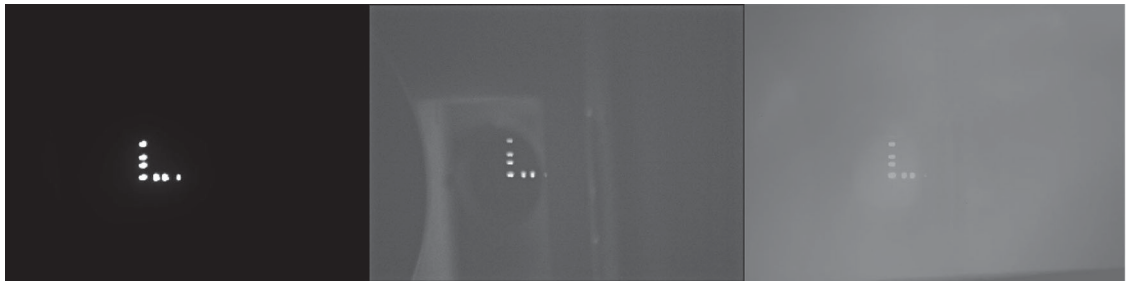

Figure 16. Calibration results of the common aperture multispectral optical system with multi-spectrum bands (VIS, SWIR, and MWIR).

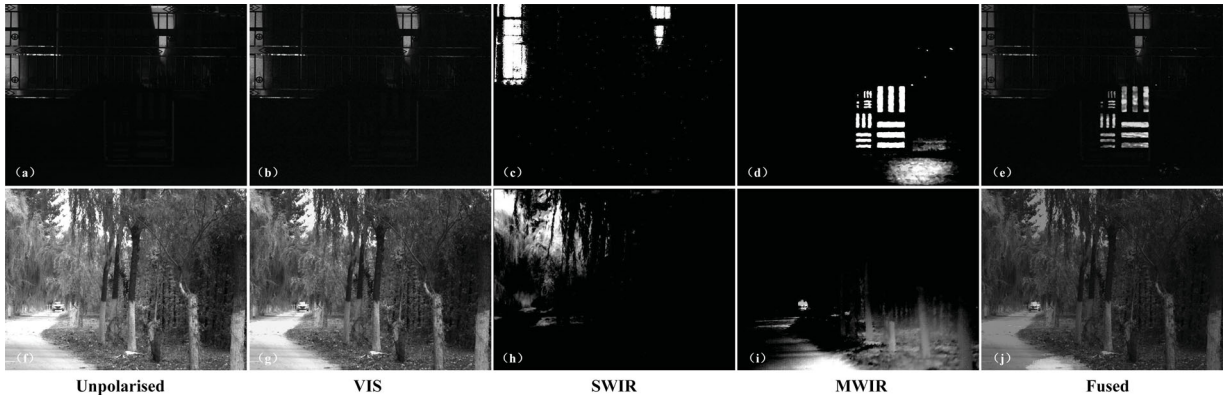

Figure 17. Multispectral (VIS, SWIR and MWIR) imaging results for original and processing pictures on different targets in complicated backgrounds. (a–e) The multispectral original and polarization process imaging experimental results for the optical resolution target at 100 m with distances and night; (f–j) The multispectral original and polarization imaging experimental results for the car at 1300 m distances in the forest.

17(g) shows the visible spectral image of the polarization fused. Figure 17(h) shows the SWIR image single-spectral fused to restrain the background information, and Figure 17(i) indicates the MWIR image as the high-light information for the final fusion. Figure 17(j) demonstrates the fusion algorithm's multispectral polarization fusion image (Section 2). According to Figure 17(j,f), the fusion image presents the same clear outline and polarization details as a VIS camera does and the same infrared polarization characteristics as an MWIR camera does and reduces the interference of background information. Figure 17(f–j) indicates the final multispectral- and polarization-fused images retain the high spatial frequency of the visible light image and the infrared feature of the medium wave infrared image. The background information is filtered by a short-wave image, making the medium wave information purer and reducing interference.

As shown above, the common-aperture multispectral polarization camera can give full play to the advantages of the VIS band, SWIR waveband and MWIR band to detect and identify the object at a distance in several complicated environments at different times. It can also identify the targets in different backgrounds by the polarization image fusion method. However, the polarization defogging algorithm cannot distinguish the target's background when dealing with a background with high brightness. It provides an insight for the subsequent research on polarization image fusion algorithm. Furthermore, more spectral-waveband can be used for future observation.

5. Conclusion

In this study, we proposed a common-aperture multispectral polarization imaging system with wider FOV. The basic principle of the whole optical system is presented in Section 2. Rather than the systems employing two spectral channels, this device utilises an on-axis common-aperture optical system to integrate three wavebands at VIS, SWIR and MWIR for detection. In the structure, we adopted two dichroic mirrors to split the different spectral light. The first dichroic mirror is used to split the incoming light into visible and infrared light. The second dichroic mirror is used to split the refracted

infrared light into SWIR and MWIR light. This system can polarize imaging on four polarization states at 0°, 45°, 90° and 135°, which can simultaneously acquire the spatial, spectral and polarization information of an object. Finally, the device is used for imaging different objects in the complicated background at different times. The polarization dehazing and multispectral fusion algorithms are adopted to increase the device images' contrast and resolution. The fusion images present a better spatial frequency, infrared and polarization characteristics are compared with those original images. The algorithm for polarization fusion image processing can be introduced into a multi-polarization optical system for contrast enhancement in future research. The experimental results verify that the common-aperture multispectral polarization camera can be highly conducive to improving object target recognition accuracy in different backgrounds and times and simplifying fusion processing algorithm, enabling better detection and recognition of distance targets in complex environments.

Acknowledgements

We gratefully acknowledge the COCO dataset.

Disclosure statement

No potential conflict of interest was reported by the author(s).

Funding

The work is supported by the Open Fund of State Key Laboratory of Applied Optics (No.SKLA0202001A05).

References

[1] He X, Liu Y, Ganesan K, et al. A single sensor based multispectral imaging camera using a narrow spectral band colour mosaic integrated on the monochrome CMOS image sensor. APL Photonics. 2020;5(4):046104.
[2] Shuji O. Snapshot multispectral imaging using a pixel-wise polarization color image sensor. Opt Express. 2020;28(33):34536–34573.
[3] Parsa O, Mohamadreza N, Mamadou D, et al. Single-shot detection of 8 unique monochrome fringe patterns respresenting 4 distinct directions via multispectral fringe projection profilometry. Sci Rep. 2021;11(1):10367.
[4] Pan Z, Shen HL. Multispectral image super-resolution via RGB image fusion and radiometric calibration. IEEE Trans Image Process. 2019;28(4):1783–1797.
[5] Mahmoud A, Xu D, Xu L. SPIE Asia-Pacific remote sensing. New Delhi; 2016. p. 6.
[6] Tyo JS, Goldstein DL, Chenault DB, et al. Review of passive imaging polarimetry for remote sensing applications. Appl. Opt. 2006;45(22):5453–5469.
[7] Liu X, Chang J, Zhong Y, et al. Optical design of a simultaneous polarization and multispectral imaging system with a common aperture. J Mod Opt. 2020;67(5):462–468.
[8] Pacheco S, Liang Rg. Snapshot, reconfigurable multispectral and multi-polarization telecentric imaging system. Opt Express. 2014;22(13):16377–16385.
[9] Scott Tyo J. Hybrid division of aperture/division of a focal-plane polarimeter for real-time polarization imagery without an instantaneous field-of-view error. Opt. Lett. 2006;31(20):2984–2986.
[10] Antonia L, Harper DJ, Marco A, et al. Spectroscopic imaging with spectral domain visible light optical coherence microscopy in Alzheimer's disease brain samples. Biomed Opt Express. 2017;8(9):4007–4025.
[11] Liu X, Chang J, Feng S, et al. Optical design of common-aperture multispectral and polarization optical imaging system with wide field of view. Chin Phys B. 2019;28(8):084201.
[12] Liu X, Chang J, Chen WL, et al. A dynamic foveated infrared imager for surveillance. Opt Lasers Eng. 2019;124:1052825.
[13] Shinoda K, Ohtera Y, Hasegawa M. Snapshot multispectral polarization imaging using a photonic crystal filter array. Opt Express. 2018;26(12):15948–15961.
[14] Zhao HJ, Li YS, Jia GR, et al. Comparing analysis of multispectral and polarimetric imaging for mid-infrared detection blindness condition. Appl. Opt. 2018;57(24):6840–6850.
[15] Mathews SA. Design and fabrication of a low-cost, multispectral imaging system. Appl Opt. 2008;47(28):71–76.
[16] Zhang JC, Luo HB, Hui B, et al. Image interpolation for division of focal plane polarimeters with intensity correlation. Opt Express. 2016;24(18):20799–20807.
[17] Zhang S, Kim M-H, Airta F, et al. High efficiency near diffraction-limited mid-infrared flat lenses based on metasurface reflectarrays. Opt Express. 2016;24(16):18024–18034.
[18] Knitter S, Hellwig T, Kues M, et al. Spectrally resolving single-shot polarimeter. Opt Lett. 2011;36(16):3048–3050.
[19] Fang S, Xia XS, Huo X, et al. Image dehazing using polarization effects of objects and airlight. Opt Express. 2014;22(16):19523–19537.
[20] Zhao Y, Zhang L, Zhang D, et al. Object separation by polarimetric and spectral imagery fusion. Comput Vis Image Underst. 2009;113(8):855–866.
[21] Fu C, Arguello H, Sadler BM, et al. Compressive spectral polarization imaging by a pixelized polarizer and colored patterned detector. J Opt Soc Am A. 2015;32(11):2178–2188.
[22] He H, Ji Y, Zhou J, et al. Optical design of decentred aperture-divided polarization imaging system. Acta Optical Sinca. 2013;33(6):0622005.
[23] Wang Q, Shi J, Wang J, et al. Design and characterization of an AOTF hyper-spectral polarization imaging system. J Mod Opt. 2016;64(1):1–7.
[24] Gao L, Kester RT, Tkaczyk TS. Compact image slicing spectrometer (iss) for hyperspectral fluorescence microscopy. Opt Express. 2009;17(15):12293–12308.
[25] Shu JLI, Jiang HL, Zhu JP, et al. Development status and key technologies of polarization imaging detection. Chin Opt. 2013;6(6):803–809.
[26] Harnett CK, Craighead HG. Liquid-crystal micropolarizer array for polarization-difference imaging. Appl Opt. 2002;41(7):1291–1296.

[27] Schechner YY, Narasimhan SG, Nayar SK. Instant dehazing of images using polarization. Proceedings of the IEEE Conference on Computer Vision and Pattern Recognition; 2001. p. 325–332.
[28] Schechner YY, Narasimhan SG, Nayar SK. Polarization-based vision through haze. Appl Opt. 2003;42(3):511–525.
[29] Namer E, Schechner YY. Advanced visibility improvement based on polarization filtered images. Proc SPIE. 2005;5888:36–45.
[30] Shwartz S, Namer E, Schechner YY. Blind haze separation. Proceedings of the IEEE Conference on Computer Vision and Pattern Recognition; 2006. p. 1984–1991.
[31] Ye S, Ma Y, Zhang Y, et al. Research on camouflage target recognition method based on polarization fusion. Laser J. 2020;41(10):25–28.
[32] Thompson NA. Optical design of common aperture, common focal plane, multispectral optics for military applications. Opt Eng. 2013;52(6):061308.